ACS OMEGA

http://pubs.acs.org/journal/acsodf

Article

The SWSe-BP vdW Heterostructure as a Promising Photocatalyst for Water Splitting with Power Conversion Efficiency of 19.4%

Jiarui Tu, Wenjun Wu, Xueling Lei,* and Pengfei Li*

Cite This: *ACS Omega* 2022, 7, 37061−37069

Read Online

ACCESS | Metrics & More | Article Recommendations

ABSTRACT: Hydrogen generation by photocatalytic water splitting has drawn enormous research attention for converting sunlight and water into clean and green hydrogen fuel. However, the search for a high efficiency photocatalyst for water splitting is a key challenge. Two dimensional (2D) van der Waals (vdW) heterostructures as photocatalysts exhibit many advantages over the stacked original materials. In this article, we designed two novel 2D vdW heterostructures composed of WSSe and blue phosphorene (BP) monolayers, SWSe-BP and SeWS-BP, which are thermodynamically stable at room temperature. Using first-principles calculations, we found that the SWSe-BP vdW heterostructure can act as a potential photocatalyst for water splitting due to its robust stabilities, type-II band alignment, moderate bandgap, and suitable band edge positions for the redox reactions of water splitting, strong optical absorption, and excellent power conversion efficiency (PCE). Remarkably, the PCE of the SWSe-BP vdW heterostructure can achieve approximately 19.4% under a 3% biaxial tensile strain.

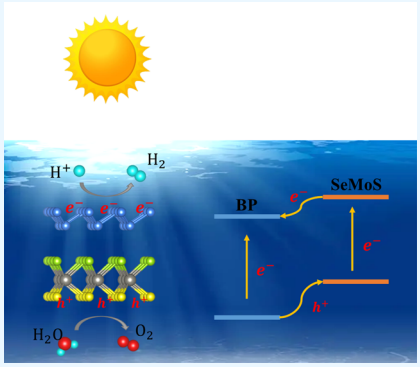

1. INTRODUCTION

To solve the worldwide energy and environmental issues, one of the effective ways is to develop renewable clean energy. For example, converting the inexhaustible solar energy into green H_2 fuel is a wise strategy.[1] However, the key challenge of this promising technology is to develop highly efficient photocatalysts for hydrogen production to improve the utilization efficiency of solar photons. Therefore, finding an efficient photocatalyst with excellent optical adsorption and high power conversion efficiency (PCE) is essential for water splitting. Two-dimensional (2D) materials have been proven to be excellent photocatalysts for water splitting due to their large surface-to-volume ratio, short carrier migration distance, and abundant active sites.[2−6] Typically, $PdSeO_3$ monolayer,[7] Janus monolayer,[8,9] and covalent organic frameworks (COFs)[10] have been predicted as the potential candidates of photocatalysts for water splitting. Recently, a new family of 2D vdW heterostructure photocatalysts has been reported and immediately garnered much attention due to its type-II band alignment, suitable band edge positions, and strong optical absorption.[11−22]

Janus monolayer, WSSe, is predicted to have suitable band alignments and excellent light adsorption.[23,24] More recently, the WSSe monolayer has also been predicted to be a promising photocatalyst for overall water splitting.[8] On the other hand, blue phosphorene (BP) has been successfully synthesized experimentally by epitaxial growth[25] and then quickly has attracted much attention. A large number of studies have shown that BP has excellent electronic and transport properties.[26−29] Especially, BP-based vdW heterostructures have been extensively investigated to extend its applications.[19,30−32] For example, the maximum PCE of the $MoSe_2$/BP and MoSSe/BP vdW heterostructures has recently been predicted to achieve 14.3% and 12.9%, respectively.[13,32]

Apart from the normal advantages of 2D materials, the 2D vdW heterostructures may generate more fascinating properties than those of the original 2D materials; e.g., a 2D van der Waals heterostructure may be more efficient than a single semiconductor as the photocatalyst used for water splitting, because the oxidation and reduction reactions of water splitting will take place in different material layers, which will prevent the reverse reaction of water decomposition.[33] Therefore, in this work, the WSSe/BP heterostructures have been designed, and the stacking mode, electronic, and optical properties have been studied by first-principles calculations. We found that the SWSe-BP heterostructure exhibits an excellent photocatalytic water splitting performance with suitable energy gap and band edge positions and remarkable optical absorption and solar-to-hydrogen energy conversion efficiency.

Received: March 31, 2022
Accepted: October 5, 2022
Published: October 14, 2022

https://doi.org/10.1021/acsomega.2c01977
ACS Omega 2022, 7, 37061−37069

2. COMPUTATIONAL DETAILS

First-principles calculations were performed by the Vienna Ab Initio Simulation Package (VASP),[34,35] and the projector augmented wave method (PAW) was used to describe the interaction between valence electrons and core ions[36,37] with the plane wave kinetic energy cutoff of 500 eV. The electron exchange-correlation energy was described by the general gradient approximation (GGA) with the Perdew−Burke−Ernzerhof (PBE) functional,[38] and the Heyd−Scuseria−Ernzerhof (HSE06) hybrid functional was chosen to further accurately assess the electronic structures.[39] All the atomic positions and the lattice parameters were fully relaxed until the total energy converged to 1×10^{-5} eV and the force on each atom was less than −0.01 eV/Å. The Monkhorst−Pack scheme was applied with a $9 \times 9 \times 1$ *k*-point mesh for the optimizations and a $18 \times 18 \times 1$ *k*-point mesh for the energy and density of states calculations.[40] A vacuum spacing of 30 Å along the *c* direction was employed to minimize the interactions between periodic images. The DFT-D3 method with Grimme correction is used to describe the long-range van der Waals (vdW) interaction between layers.[41,42] Meanwhile, a dipole correction along the vertical direction of the cell is utilized to obtain the converged electronic properties. The ab initio molecular dynamics (AIMD) simulations with a $4 \times 4 \times 1$ supercells and a $1 \times 1 \times 1$ *k*-point mesh at the Γ-point were conducted under the NVT ensemble.[43] A Verlet algorithm was integrated with Newton's equations of motion at a time step of 1 fs for a total simulation time of 6 ps.

3. RESULTS AND DISCUSSION

3.1. Geometric and Electronic Structures of Janus WSSe and BP Monolayers. First of all, the optimized geometric structures of WSSe and BP monolayers and corresponding electronic structures calculated at the HSE06 level are displayed in Figure 1. The lattice parameters, bond lengths of W−Se, W−S, and P−P, and values of the bandgap of SWSe and BP monolayers are listed in Table 1. For the Janus WSSe monolayer, the optimized lattice constant of the primitive cell is 3.25 Å, which is in good agreement with the previous calculated value of 3.26 Å.[8] Moreover, the bond lengths of W−Se and W−S are 2.54 and 2.42 Å, respectively. These results are in fair agreement with those reported values.[8] For the BP monolayer, the optimized lattice constant and P−P bond length are 3.27 and 2.26 Å, respectively, which are comparable with the previous publications.[18,25,44] In addition, Figure 1 and Table 1 show that the Janus WSSe monolayer is a direct bandgap semiconductor with HSE06 gap of 1.97 eV, while the BP monolayer is an indirect bandgap semiconductor with HSE06 gap of 2.89 eV. These calculated gaps are consistent with the previous reports.[8,18]

3.2. Geometric and Electronic Structures of the WSSe/BP vdW Heterostructures. Considering two sides of the Janus WSSe monolayer, SWSe-BP and SeWS-BP were employed to describe the primitive cell of WSSe/BP vdW heterostructures. The SWSe-BP means that the interface of the heterostructure is composed of a P atomic layer and Se atomic layer, while the SeWS-BP means that the interface of the heterostructure is composed of a P atomic layer and S atomic layer. To obtain the optimal stacking mode for the SWSe-BP and SeWS-BP vdW heterostructures, we broadly considered a variety of stacking configurations. After structural optimization, the best structure with the lowest energy is selected as the final

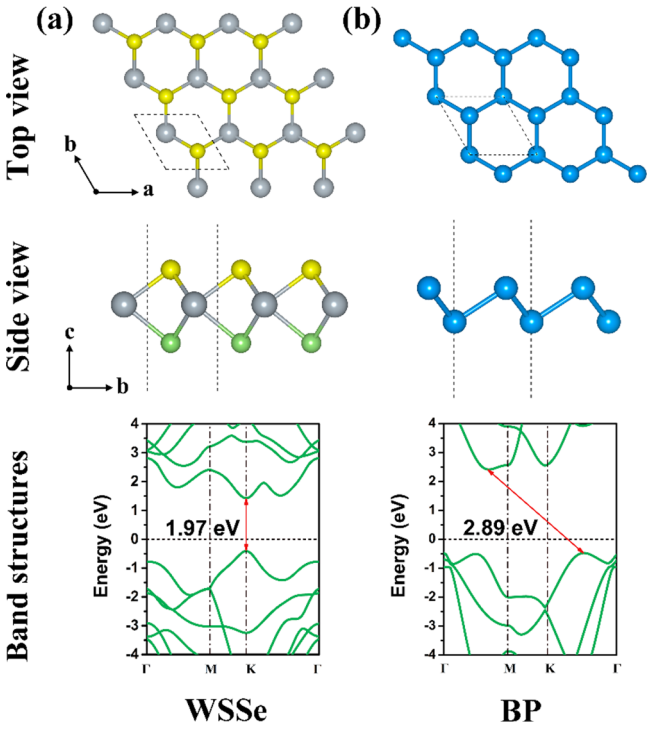

Figure 1. Top view and side view of optimized geometric structures and HSE06 band structures of WSSe (a) and BP (b) monolayers, gray, yellow, green, and blue spheres represent W, S, Se, and P atoms, respectively.

Table 1. Lattice Parameters (a); Bond Lengths of W−Se (d_{W-Se}), W−S (d_{W-S}), and P−P (d_{P-P}); and HSE06 Bandgaps of the Janus WSSe and BP Monolayers

	a (Å)	$d_{X\text{-}Se}$ (Å)	$d_{X\text{-}S}$ (Å)	d_{P-P} (Å)	E_g^{hse06} (eV)
WSSe	3.25	2.54	2.42	--	1.97
BP	3.27	--	--	2.26	2.89

structure of the SWSe-BP and SeWS-BP vdW heterostructures. As shown in Figure 2, evidently, both the SWSe-BP vdW heterostructure and the SeWS-BP vdW heterostructure, top view, show the honeycomb structure; the side view shows that

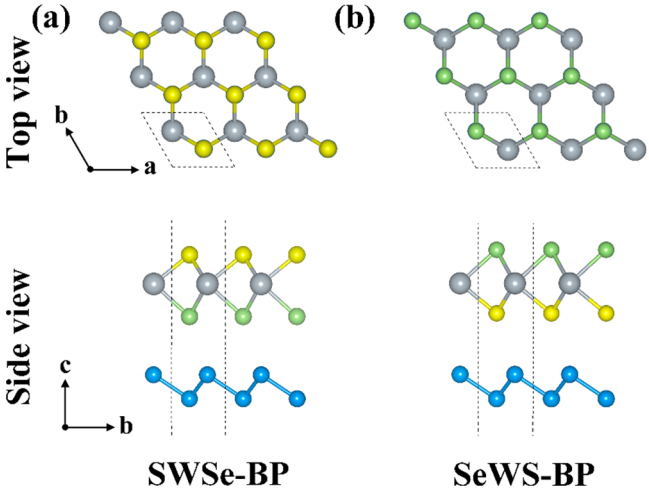

Figure 2. Top view and side view of optimized structures of the SWSe-BP (a) and SeWS-BP (b) vdW heterostructures.

https://doi.org/10.1021/acsomega.2c01977
ACS Omega 2022, 7, 37061−37069

the upper P and lower P atoms are located directly under the W atom and Se/S atom, respectively. In order to examine the stabilities of these vdW heterostructures, we further calculated the formation energy, which is defined as follows:

$$E_{form} = E_{total} - E_{WSSe} - E_{BP} \quad (1)$$

where E_{total}, E_{WSSe}, and E_{BP} are the total energy of the heterostructure, isolated WSSe and BP monolayer, respectively. A negative formation energy enables easy formation of heterostructure from the two original parts. Table 2 shows that the formation energy of the SWSe-BP and SeWS-BP vdW heterostructures are about −0.9 eV, indicating that these heterostructures can form easily and are then energetically stable. In addition, the optimized structural parameters are also listed in Table 2, from which we can see that the bond lengths of W−Se, W−S, and P−P are almost the same as they are in the separate WSSe and BP monolayers, indicating that the structures of the original parts will not be greatly affected by the formation of heterostructures. On the other hand, the layer spacing of about 3 Å in each heterostructure shows that there is indeed vdW interaction between layers.

Table 2. Bond Lengths of W−Se (d_{W-Se}), W−S (d_{W-S}) and P−P (d_{P-P}), the Distance of the Interface (d_L), the Lattice Parameters (a), and the Formation Energy (E_{form}) of the SWSe-BP and SeWS-BP vdW Heterostructures

	d_{W-Se} (Å)	d_{W-S} (Å)	d_{P-P} (Å)	d_L (Å)	a (Å)	E_{form} (eV)
SWSe-BP	2.54	2.42	2.25	3.22	3.24	−0.90
SeWS-BP	2.54	2.42	2.25	3.12	3.24	−0.89

Considering that these vdW heterostructures have not been experimentally synthesized, we carried out the AIMD simulations to examine the thermodynamic stability. The fluctuation of temperature and total energy as well as the geometric structures of the SWSe-BP and SeWS-BP vdW heterostructures are displayed in Figure 3, from which we can see that after 6 ps simulations at room temperature, the fluctuations of the total energy and temperature are very small, and the structures of the SWSe-BP and SeWS-BP vdW heterostructures have no obvious distortion, showing that the heterostructures have good thermodynamic stability at 300 K room temperature.

One of the key properties for photocatalytic water splitting is the electronic structure of the photocatalyst, which controls the first step of photocatalytic water splitting.[5] As shown in Figure 4, the weighted band structure and the projected density of states of the SWSe-BP and SeWS-BP vdW heterostructures are displayed. It should be noted that the valence band maximum (VBM) of the SWSe-BP and SeWS-BP vdW heterostructures locates at the Γ point instead of the K point, indicating that the VBM of the Janus WSSe monolayer shifts from the K point to the Γ point due to vdW interaction when forming a heterostructure. Additionally, the electronic structures of the SWSe-BP vdW heterostructure indicate that the conduction band minimum (CBM) and VBM are from the BP and Janus WSSe monolayer, respectively. Therefore, the SWSe-BP vdW heterostructure has typical type-II band structures with the indirect bandgap of 1.59 eV, which is of great significance for suppressing the recombination of photogenerated carriers, and then meeting the requirements of low exciton recombination rate as an effective photocatalyst. Leung et al.[45] reported that the bandgap of the photocatalyst must exceed the free energy of water splitting of 1.23 eV and be smaller than about 3.0 eV to enhance solar absorption. Then, our calculations show that the SWSe-BP heterostructure can enhance solar absorption as a photocatalyst, because its bandgap is in the range of 1.23−3.0 eV. On the contrary, the electronic structures of the SeWS-BP vdW heterostructure indicate that both the CBM and the VBM are from the Janus WSSe monolayer. Therefore, the SeWS-BP vdW heterostructure has type-I band structure with the indirect bandgap of 1.80 eV, and thus it is not suitable for use as a photocatalyst and is no longer considered in the following studies.

Then, we mainly discuss the electronic properties of the SWSe-BP vdW heterostructure. Due to the asymmetric structures in the vertical direction, there should be a vertical dipole in the 2D heterostructure, such as Janus structures of transition metal dichalcogenides,[46] Janus group-III monochalcogenide multilayers,[47] metal chalcogenides Janus mono-

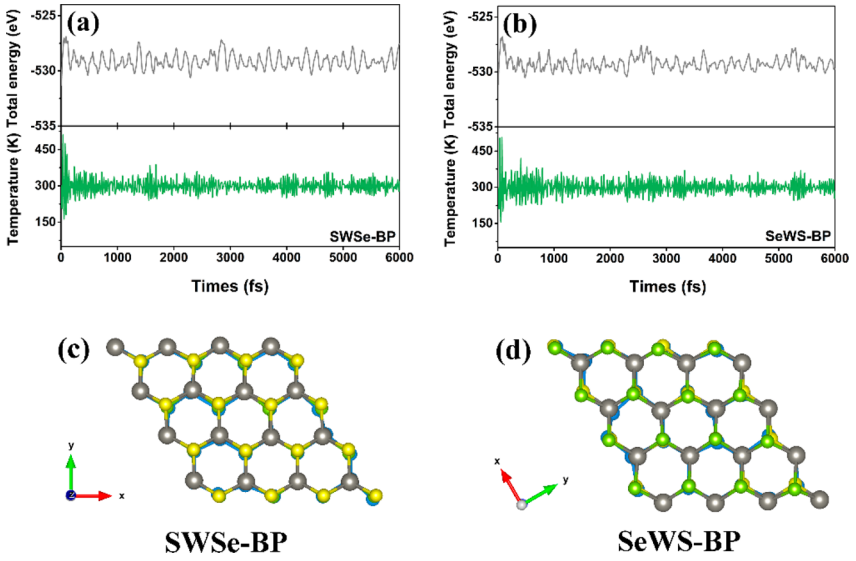

Figure 3. Fluctuation of total energy and temperature as well as the snapshots of SWSe-BP (a) and (c), SeWS-BP (b), and (d) vdW heterostructures obtained from AIMD simulations at 300 K.

https://doi.org/10.1021/acsomega.2c01977
ACS Omega 2022, 7, 37061−37069

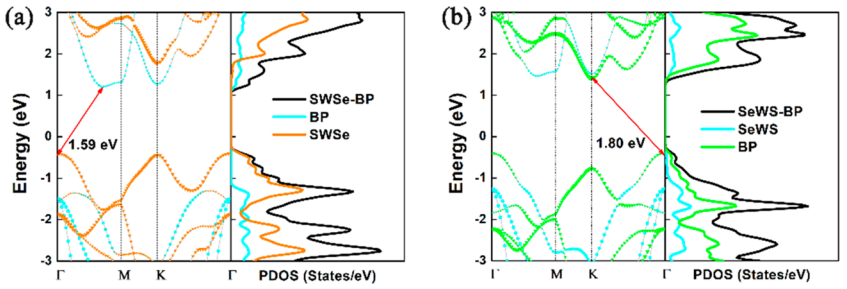

Figure 4. Weighted band structures and projected density of states of (a) SWSe-BP and (b) SeWS-BP vdW heterostructures calculated at the HSE06 level.

layers,[48] and the 2D M_2X_3 (M = Al, Ga, In; X = S, Se, Te) family.[49] For the SWSe-BP vdW heterostructure, it is found that the BP layer is positively charged and the WSSe layer is negatively charged, which leads to an intrinsic dipole of 0.15 D, which is in good agreement with that of GeSe (0.16 D).[50] This intrinsic dipole introduces an internal electric field in the direction pointing from BP surface to the WSSe surface and induces the electrostatic potential difference. Figure 5a shows

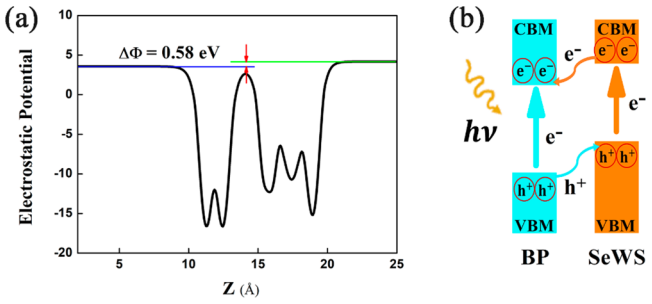

Figure 5. Electrostatic potential difference (a) and band alignment (b) of the SWSe-BP vdW heterostructure.

that the electrostatic potential difference between the WSSe layer and the BP layer in the SWSe-BP vdW heterostructure is 0.58 eV, which is enough to cause band bending across the junction surface. Figure 5b shows that the photogenerated electrons in the CBM of WSSe could transfer to the CBM of BP by the chemical potential difference of conduction band offset (CBO), while the photogenerated holes in the VBM of BP can migrate to the VBM of WSSe via the chemical potential difference of the valence band offset (VBO). Therefore, the excited electrons reside on the BP surface, while the holes stay on the WSSe surface, and the internal electric field prevents the electrons from going back to the WSSe surface. As a result, a perfect spatial separation of the photogenerated electron−hole pair can be achieved, which is consistent with the photocatalytic model proposed by Yang's group.[51] Then, the hydrogen evolution reactions (HER) will occur on the BP layer due to the accumulation of a large number of electrons, whereas the oxygen evolution reactions (OER) will occur on the WSSe layer due to the accumulation of a large number of holes. Thus, the SWSe-BP vdW heterostructure is a potential photocatalyst for overall water splitting.

3.3. Electronic Properties of the SWSe-BP vdW Heterostructure under Biaxial Strains. Bandgap engineering is always the hottest topic. Various strategies have been proposed to tailor the bandgap of materials. Typically, strain is a convenient and powerful tool to adjust the bandgap of materials. To evaluate the bandgap of the SWSe-BP vdW heterostructure under strain, we examined the electronic structures of the SWSe-BP vdW heterostructure with biaxial strains from −3% to +3% with a step of 1%. Figure 6 evidently

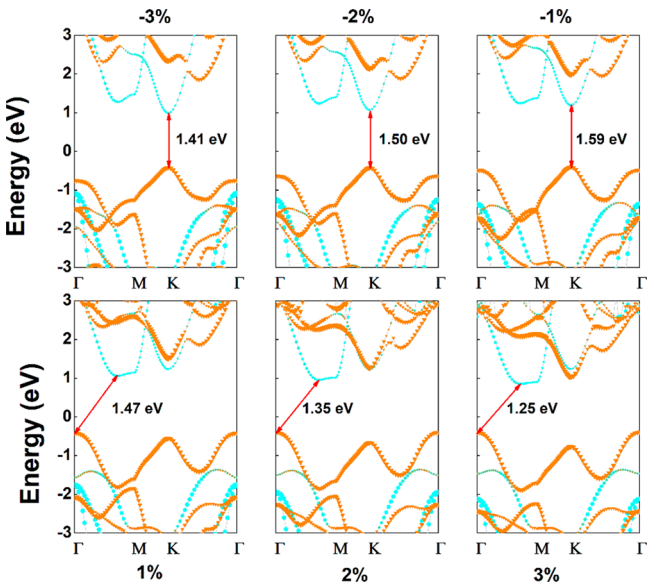

Figure 6. Weighted band structures of the SWSe-BP vdW heterostructure under strains from −3% to 3% calculated at the HSE06 level.

shows that the SWSe-BP vdW heterostructure has direct bandgap under compressive strain due to the shifts of both CBM and VBM to the K point and indirect bandgap under tensile strain. In addition, it is worth noting that the SWSe-BP vdW heterostructure still maintains the type-II band structures under up to 3% tensile strain and −3% compressive strain. Furthermore, the bandgap decreases as the strain increases. Specifically, the bandgap decreases from 1.47 to 1.25 eV under tensile strain from 1% to 3%, and decreases from 1.59 to 1.41 eV under compressive strain from −1% to −3%. Fortunately, the bandgap of 1.25 eV under 3% tensile strain is still in the 1.23−3.0 eV energy window.

In addition, for a good photocatalyst, apart from the sufficient bandgap that must be satisfied, the band edges must straddle the water redox potential. To further evaluate the photocatalytic ability, the vacuum energy level is taken as the reference, and the redox energy levels of SWSe-BP with respect to the standard water reduction (−5.76 eV) and oxidation potential levels (−4.44 eV) at PH = 0 have been aligned, as shown in Figure 7. Obviously, the VBM and CBM of SWSe-BP are located outside the reduction potential and oxidation

https://doi.org/10.1021/acsomega.2c01977
ACS Omega 2022, 7, 37061−37069

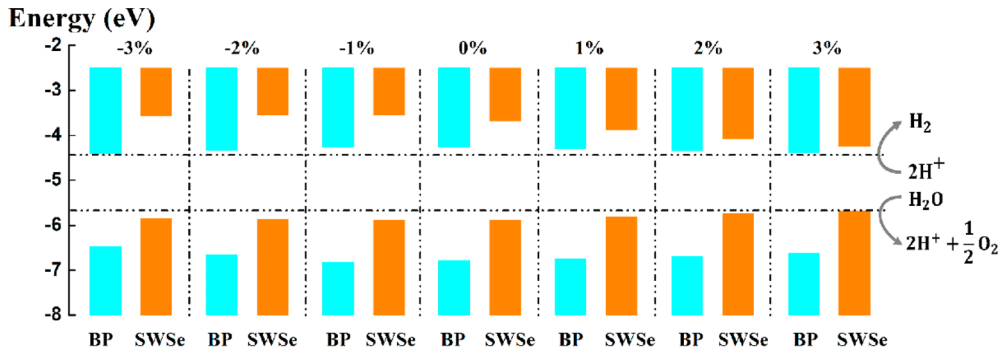

Figure 7. Band edge positions of the SWSe-BP vdW heterostructure under biaxial strains from −3% to 3% relative to the redox potential of water calculated at the HSE06 level at pH = 0.

potential of water, respectively. Specifically, the energy difference between VBM and the water oxidation potential is 0.22 eV, and the energy difference is 0.14 eV between CBM and water reduction potential, which are large enough for water splitting into H_2 and O_2. When applying a biaxial strain on the SWSe-BP heterostructure from −3% to +3%, its geometric structure has not been damaged, and the band edge positions relative to the redox potential of water are also shown in Figure 7. It is clear that the SWSe-BP vdW heterostructure could ensure a suitable band alignment under compressive strain and tensile strain up to ±3%. Moreover, the position of VBM (CBM) increases (decreases) linearly when the strain increases from 1% to 3%. The band edges of all the strained systems are proper for the photocatalytic redox reactions of water, indicating that a strain tolerance of the photocatalytic water splitting abilities.

3.4. Optical Properties of the SWSe-BP vdW Heterostructure under Biaxial Strains. In order to evaluate the utilization efficiency of sunlight, we also calculated the power conversion efficiency (PCE) of the SWSe-BP vdW heterostructure under strains from −3% to 3% at the HSE06 level, which was developed by Scharber et al.[52,53]

$$\eta = \frac{\beta_{FF} J_{sc} V_{oc}}{P_{solar}} = \frac{0.65(E_g^d - \Delta E_c - 0.3)\int_{E_g^d}^{\infty} \frac{P(\hbar\varpi)}{\hbar\varpi}\, d(\hbar\varpi)}{\int_0^{\infty} P(\hbar\varpi)\, d(\hbar\varpi)} \quad (2)$$

where the band-fill factor β_{FF} is assumed to be 0.65, J_{sc} is short circuit current expressed as $(E_g^d - \Delta E_c - 0.3)$, in which E_g^d and ΔE_c are the bandgap of the donor and the CBO, respectively. V_{OC} is the open circuit voltage expressed as $\int_{E_g}^{\infty} \frac{P(\hbar\varpi)}{\hbar\varpi}\, d(\hbar\varpi)$, in which $P(\hbar\varpi)$ is the AM 1.5 G solar flux at the photon energy $\hbar\varpi$. P_{solar} is the total incident solar power per unit area equal to $\int_0^{\infty} P(\hbar\varpi)\, d(\hbar\varpi)$. The values of CBM, VBM, bandgaps, bandgaps of the donor, CBO, and PCE of the SWSe-BP vdW heterostructure under strains from −3% to 3% are summarized in Table 3. It is clear that the PCE of the SWSe-BP vdW heterostructure decreases under the compressive strain, while it increases under the tensile strain. Specifically, the SWSe-BP vdW heterostructure without any strain has a PCE of ∼9.1%, which is comparable to the proposed PCBM/$C_1(BN)_7$ (11%),[52] Al_2C/ZnO (12.6%),[54] AsP/CdSe heterostructure (13%),[55] and recently predicted MoSSe/BP heterostructure (12.9%)[13] Remarkably, the PCE of the SWSe-BP vdW heterostructure can be enhanced to ∼19.4% under a 3% tensile strain, as shown in Figure 8a.

Table 3. CBM, VBM, Bandgaps (E_g^{HSE}), Bandgaps of the Donor (E_g^d), CBO (ΔE_c), and PCE under Strains from −3% to 3%

Strain (%)	CBM (eV)	VBM (eV)	E_g^{HSE}(eV)	E_g^d (eV)	ΔE_c (eV)	PCE (%)
−3	0.99	−0.42	1.41	2.27	0.86	6.8
−2	1.07	−0.42	1.50	2.31	0.81	6.9
−1	1.19	−0.40	1.59	2.35	0.76	6.9
0	1.17	−0.42	1.59	2.19	0.60	9.1
1	1.06	−0.41	1.47	1.93	0.46	12.4
2	0.96	−0.40	1.35	1.63	0.28	16.8
3	0.86	−0.40	1.25	1.44	0.18	19.4

Besides, the ability to utilize visible light is one of the important requirements for a 2D vdW heterostructure as a photocatalyst. Therefore, we calculated the absorption coefficient of the SWSe-BP vdW heterostructure under biaxial tensile strain (0%, 1%, 2%, and 3%) using the HSE06 method, which is defined as[8]

$$\alpha(\omega) = \frac{\sqrt{2}\,\omega}{c}\left[\sqrt{\varepsilon_1^2(\omega) + \varepsilon_2^2(\omega)} - \varepsilon_1(\omega)\right]^{1/2} \quad (3)$$

where ω is the angular frequency, c is the speed of light in vacuum, and ε_1 and ε_2 are the real and imaginary parts of the dielectric function, respectively. The optical absorption spectrum for the SWSe-BP vdW heterostructure under biaxial tensile strain are shown in Figure 8b, from which we can see that the SWSe-BP vdW heterostructure under tensile strain of 0%, 1%, 2%, and 3% has an absorption peak in the visible light and near-ultraviolet light regions, which can greatly improve the utilization of sunlight. The maximum absorption intensities are 3.40×10^5/cm, 3.98×10^5/cm, 3.68×10^5/cm, and 3.56×10^5/cm for 0%, 1%, 2%, and 3% tensile strain, respectively; corresponding wavelengths are 394.2 nm, 358.0 nm, 376.5 nm, and 406 nm, respectively. Therefore, the SWSe-BP vdW heterostructure is an efficient light harvesting photocatalyst.

To deeply understand the photocatalytic mechanism and higher PCE under tensile strain, we further examined the project density of states of the SWSe-BP vdW heterostructure under strains of 0%, 1%, 2%, and 3%. As shown in Figure 9, with the increase of the tensile strain from 0% to 3%, the lowest unoccupied orbitals of the W atom rapidly decrease, whereas the lowest unoccupied orbitals of S/Se atoms decrease very slowly. Therefore, the CBM of SWSe is mainly contributed by a W atom. Moreover, the lowest unoccupied orbitals of the W atom approach that of a P atom under a 3% tensile strain, which results in the small value of CBO (0.18

https://doi.org/10.1021/acsomega.2c01977
ACS Omega 2022, 7, 37061−37069

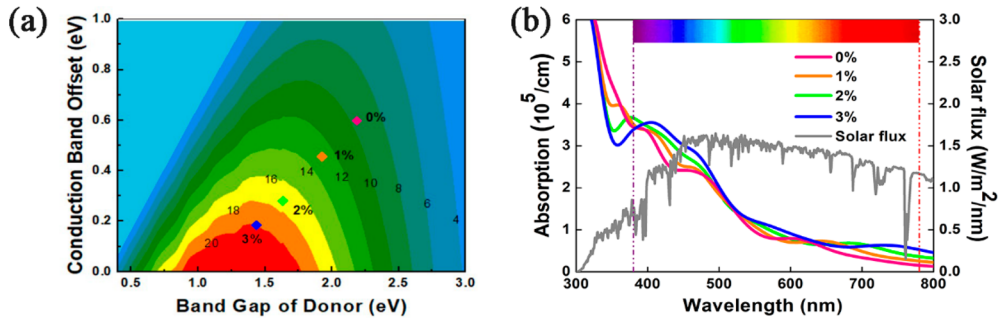

Figure 8. (a) PCE contour and (b) optical absorption of the SWSe-BP vdW heterostructure under biaxial tensile strain of 0%, 1%, 2%, and 3% calculated at the HSE06 level.

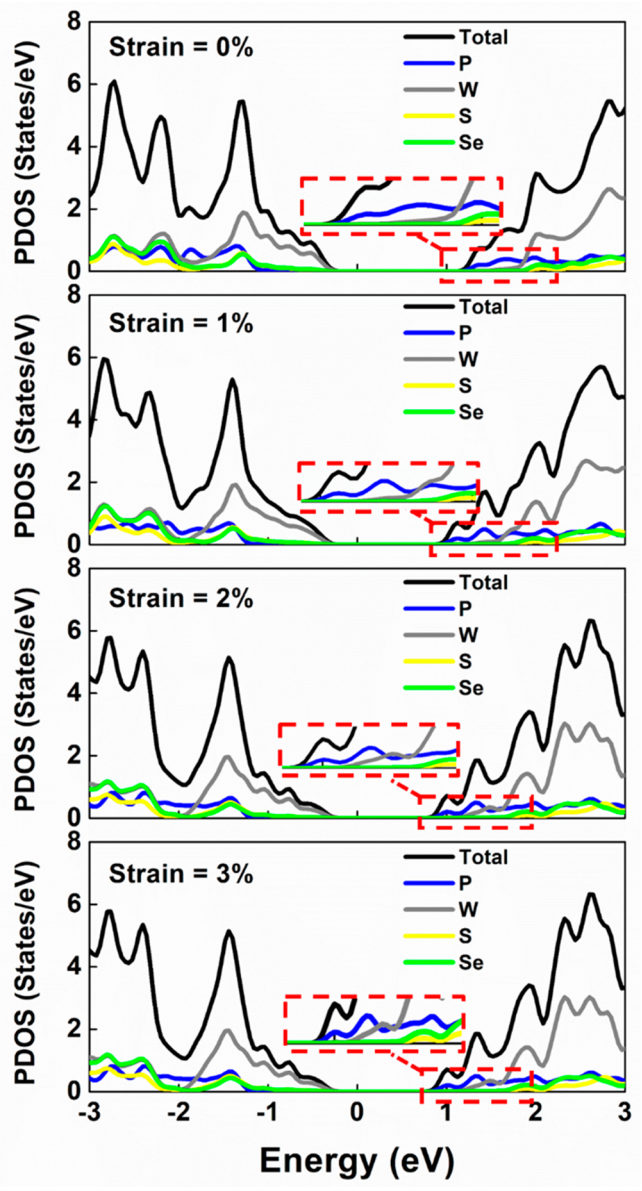

Figure 9. Projected density of states (PDOS) of the SWSe-BP vdW heterostructure under strains of 0%, 1%, 2%, and 3%.

eV) causing the high PCE value. On the other hand, with the increase of the tensile strain, the bandgap of the donor (WSSe) also decreases due to the decrease of the lowest unoccupied orbitals of the W atom. Specifically, the bandgap of the donor decreased to 1.44 eV under a 3% tensile strain. Therefore, both the CBO and the bandgap of the donor are decreased with increasing tensile strain due to the decrease of the lowest unoccupied orbitals of W, and they are two critically important factors for PCE value.

3.5. Gibbs Free Energy Profiles for HER and OER. The HER and OER catalytic activity is critically important for overall water splitting photocatalysts, which can be evaluated by the Gibbs free energy change of each step for HER and OER.[56] Since the CBM and VBM of the SWSe-BP vdW heterostructure are mainly contributed by the BP and SWSe layer, respectively, the HER performance on BP layer and the OER catalytic activity on SWSe layer are examined. For HER, three hydrogen adsorption sites including top site, bridge site, and hollow site have been considered, and results show that the hydrogen atom adsorbed on the top of P atom is the most stable in thermodynamics, with the H−P bond length of 1.44 Å, as shown in the inset of Figure 10a. Using the standard hydrogen electrode (SHE) as the reference, the Gibbs free energy with different hydrogen coverages on BP layer is shown in Figure 10a, from which we can see that the ΔG of the third hydrogen could achieve as low as 0.42 eV, indicating that the SWSe-BP vdW heterostructure is a potential catalyst for the HER at an appropriate H coverage.

Then the OER performance on the SWSe layer was evaluated, and the Gibbs free energy of each elementary reaction (ΔG_1−ΔG_4) was calculated. The overall Gibbs free energy profiles for OER elementary reaction steps at external potential (U = 0 V), equilibrium potential (U = 1.23 V), and the potential of the VBM relative to the SHE (U = 1.64 V) under the extreme conditions of pH = 0 are shown in Figure 10b. Obviously, at U = 0 V, ΔG of the first three steps is positive, while the last step is negative, and the first step is the rate-determining step with ΔG_1 of 2.57 eV. The largest ΔG for the first step indicates that the dissociation of H_2O to OH* is hindered and leads to sluggish OER kinetics. At the equilibrium potential of water oxidation U = 1.23 V, the first and third steps are uphill, while the second and last steps are downhill. The ΔG_1 of the rate-determining step will decrease to 1.34 eV, which is comparable to that of many TM@C catalysts or metal oxides.[57] When an operating potential of 1.64 V is applied, the ΔG_1 and ΔG_3 are less positive and ΔG_2 and ΔG_4 are more negative, the ΔG_1 of the rate-determining step will then continue to decrease to 0.93 eV. This indicates that the OER becomes easier under the driving force of the VBM of the SWSe-BP vdW heterostructure.[58,59]

It is noted that in the present work, we have only evaluated the possibility of a defect-free SWSe-BP vdW heterostructure

https://doi.org/10.1021/acsomega.2c01977
ACS Omega 2022, 7, 37061−37069

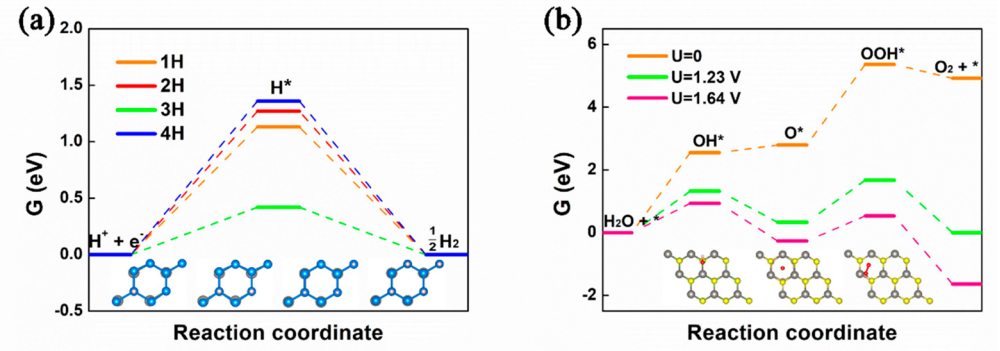

Figure 10. Gibbs free energy (G) profiles for HER process on the BP layer (a) and the OER process on the SWSe layer (b) at pH = 0. 1H, 2H, 3H, and 4H represent different H coverages.

as a photocatalyst for water splitting. However, the PCE of 19.4% may be challenging to reproduce with a defect heterostructure, and it is unknown whether the defects will render the heterostructure unsuitable for photocatalyst, and the effects of defects on the stability and electronic structure of heterostructure need to be further evaluated. Providing that the defects are crucially significant to the heterostructure as a photocatalyst for water splitting, undoubtedly, more efforts need to be made to study these issues in the future. Simultaneously, the role the defects play in the heterostructure are of great value in scientific research, which makes it worthwhile to conduct a series of experiments coupled with simulations.

4. CONCLUSIONS

In summary, we systematically investigated the structural, electronic, and optical properties of the SWSe-BP and SeWS-BP vdW heterostructures by first-principles calculations. The negative formation energies (about −0.9 eV) and AIMD simulations show that the two vdW heterostructures are energetically stable and have thermodynamic stabilities. The calculated electronic structures indicate that the SWSe-BP vdW heterostructure is a type-II band alignment semiconductor with indirect bandgap of 1.59 eV; the VBM and CBM are from the WSSe and BP monolayer, respectively. However, the SeWS-BP vdW heterostructure is a type-I band alignment semiconductor with indirect bandgap of 1.80 eV. In addition, the bandgaps of the SWSe-BP vdW heterostructure under strains from −3% to 3% are examined, which exceed the free energy of water splitting of 1.23 eV and smaller than 3 eV, indicating that the SWSe-BP vdW heterostructure under strains up to ±3% can enhance sunlight absorption as photocatalysts. Furthermore, the calculated band edge energies show that the band edge positions of the SWSe-BP vdW heterostructure under strains up to ±3% straddle the redox potentials of water, indicating that they can act as an effective photocatalyst for water splitting. Besides, the SWSe-BP vdW heterostructure has strong optical absorption in the near-UV and visible light, and possess significantly high PCE, e.g., ∼9.1% for the SWSe-BP vdW heterostructure and extraordinarily high PCE of ∼19.4% under a 3% tensile strain. In short, the results of our calculations evidenced that the SWSe-BP vdW heterostructure can be considered a promising photocatalyst for water splitting due to its type-II band alignment, suitable energy gap, band edge positions, remarkable optical absorption, and solar-to-hydrogen energy conversion efficiency.

AUTHOR INFORMATION

Corresponding Authors

Xueling Lei − *Department of Physics, Jiangxi Normal University, Nanchang, Jiangxi 330022, China;* orcid.org/0000-0002-2482-3728; Email: xueling@mail.ustc.edu.cn

Pengfei Li − *Key Laboratory of Materials Physics and Anhui Key Laboratory of Nanomaterials and Nanotechnology, Institute of Solid State Physics, Hefei Institutes of Physical Science, Chinese Academy of Sciences, Hefei 230031, China;* Email: pfli@issp.ac.cn

Authors

Jiarui Tu − *Department of Physics, Jiangxi Normal University, Nanchang, Jiangxi 330022, China*

Wenjun Wu − *Department of Physics, Jiangxi Normal University, Nanchang, Jiangxi 330022, China*

Complete contact information is available at: https://pubs.acs.org/10.1021/acsomega.2c01977

Notes

The authors declare no competing financial interest.

ACKNOWLEDGMENTS

The authors thank the Natural Science Foundation of China (Grant Nos. 12164020) and the Natural Science Foundation of Jiangxi Province (Grant No. 20202BAB201012) for financial support of the current work. We gratefully acknowledge Hefei Advanced Computing Center for computational support.

REFERENCES

(1) Ran, J.; Qu, J.; Zhang, H.; Wen, T.; Wang, H.; Chen, S.; Song, L.; Zhang, X.; Jing, L.; Zheng, R.; Qiao, S. Z. 2D Metal Organic Framework Nanosheet: A Universal Platform Promoting Highly Efficient Visible-Light-Induced Hydrogen Production. *Adv. Energy Mater.* **2019**, *9* (11), 1803402.

(2) Jariwala, D.; Sangwan, V. K.; Lauhon, L. J.; Marks, T. J.; Hersam, M. C. Carbon nanomaterials for electronics, optoelectronics, photovoltaics, and sensing. *Chem. Soc. Rev.* **2013**, *42* (7), 2824−2860.

(3) Li, S.-L.; Tsukagoshi, K.; Orgiu, E.; Samorì, P. Charge transport and mobility engineering in two-dimensional transition metal chalcogenide semiconductors. *Chem. Soc. Rev.* **2016**, *45* (1), 118−151.

(4) Xu, L.; Huang, W.-Q.; Wang, L.-L.; Tian, Z.-A.; Hu, W.; Ma, Y.; Wang, X.; Pan, A.; Huang, G.-F. Insights into Enhanced Visible-Light Photocatalytic Hydrogen Evolution of g-C3N4 and Highly Reduced Graphene Oxide Composite: The Role of Oxygen. *Chem. Mater.* **2015**, *27* (5), 1612−1621.

(5) Singh, A. K.; Mathew, K.; Zhuang, H. L.; Hennig, R. G. Computational Screening of 2D Materials for Photocatalysis. *J. Phys. Chem. Lett.* **2015**, *6* (6), 1087−1098.
(6) Zhuang, H. L.; Hennig, R. G. Single-Layer Group-III Monochalcogenide Photocatalysts for Water Splitting. *Chem. Mater.* **2013**, *25* (15), 3232−3238.
(7) Qiao, M.; Liu, J.; Wang, Y.; Li, Y.; Chen, Z. PdSeO3Monolayer: Promising Inorganic 2D Photocatalyst for Direct Overall Water Splitting Without Using Sacrificial Reagents and Cocatalysts. *J. Am. Chem. Soc.* **2018**, *140* (38), 12256−12262.
(8) Ju, L.; Bie, M.; Tang, X.; Shang, J.; Kou, L. Janus WSSe Monolayer: An Excellent Photocatalyst for Overall Water Splitting. *ACS Appl. Mater. Interfaces* **2020**, DOI: 10.1021/acsami.0c06149.
(9) Lei, X.; Ouyang, C.; Huang, K. A first-principles investigation of Janus MoSSe as a catalyst for photocatalytic water-splitting. *Appl. Surf. Sci.* **2021**, *537*, 147919.
(10) Wan, Y.; Wang, L.; Xu, H.; Wu, X.; Yang, J. A Simple Molecular Design Strategy for Two-Dimensional Covalent Organic Framework Capable of Visible-Light-Driven Water Splitting. *J. Am. Chem. Soc.* **2020**, *142* (9), 4508−4516.
(11) Chiu, M.-H.; Zhang, C.; Shiu, H.-W.; Chuu, C.-P.; Chen, C.-H.; Chang, C.-Y. S.; Chen, C.-H.; Chou, M.-Y.; Shih, C.-K.; Li, L.-J. Determination of band alignment in the single-layer MoS2/WSe2 heterojunction. *Nat. Commun.* **2015**, *6* (1), 1 DOI: 10.1038/ncomms8666.
(12) Rivera, P.; Schaibley, J. R.; Jones, A. M.; Ross, J. S.; Wu, S.; Aivazian, G.; Klement, P.; Seyler, K.; Clark, G.; Ghimire, N. J.; Yan, J.; Mandrus, D. G.; Yao, W.; Xu, X. Observation of long-lived interlayer excitons in monolayer MoSe2−WSe2 heterostructures. *Nat. Commun.* **2015**, *6* (1), 1 DOI: 10.1038/ncomms7242.
(13) Luo, Y.; Wang, S.; Shu, H.; Chou, J.-P.; Ren, K.; Yu, J.; Sun, M. A MoSSe/blue phosphorene vdw heterostructure with energy conversion efficiency of 19.9% for photocatalytic water splitting. *Semicond. Sci. Technol.* **2020**, *35* (12), 125008.
(14) Ren, K.; Luo, Y.; Wang, S.; Chou, J. P.; Yu, J.; Tang, W.; Sun, M. A van der Waals Heterostructure Based on Graphene-like Gallium Nitride and Boron Selenide: A High-Efficiency Photocatalyst for Water Splitting. *ACS Omega* **2019**, *4* (26), 21689−21697.
(15) Xu, L.; Huang, W.-Q.; Hu, W.; Yang, K.; Zhou, B.-X.; Pan, A.; Huang, G.-F. Two-Dimensional MoS2-Graphene-Based Multilayer van der Waals Heterostructures: Enhanced Charge Transfer and Optical Absorption, and Electric-Field Tunable Dirac Point and Band Gap. *Chem. Mater.* **2017**, *29* (13), 5504−5512.
(16) Long, C.; Dai, Y.; Gong, Z. R.; Jin, H. Robust type-II band alignment in Janus-MoSSe bilayer with extremely long carrier lifetime induced by the intrinsic electric field. *Phys. Rev. B* **2019**, *99* (11), 7.
(17) Shang, C.; Xu, B.; Lei, X.; Yu, S.; Chen, D.; Wu, M.; Sun, B.; Liu, G.; Ouyang, C. Bandgap tuning in MoSSe bilayers: synergistic effects of dipole moment and interlayer distance. *Phys. Chem. Chem. Phys.* **2018**, *20* (32), 20919−20926.
(18) Chen, D.; Lei, X.; Wang, Y.; Zhong, S.; Liu, G.; Xu, B.; Ouyang, C. Tunable electronic structures in BP/MoSSe van der Waals heterostructures by external electric field and strain. *Appl. Surf. Sci.* **2019**, *497*, 143809.
(19) Wang, B.-J.; Li, X.-H.; Cai, X.-L.; Yu, W.-Y.; Zhang, L.-W.; Zhao, R.-Q.; Ke, S.-H. Blue Phosphorus/Mg(OH)2 van der Waals Heterostructures as Promising Visible-Light Photocatalysts for Water Splitting. *J. Phys.Chem. C* **2018**, *122* (13), 7075−7080.
(20) Shahid, I.; Ahmad, S.; Shehzad, N.; Yao, S.; Nguyen, C. V.; Zhang, L.; Zhou, Z. Electronic and photocatalytic performance of boron phosphide-blue phosphorene vdW heterostructures. *Appl. Surf. Sci.* **2020**, *523*, 146483.
(21) Shehzad, N.; Shahid, I.; Yao, S.; Ahmad, S.; Ali, A.; Zhang, L.; Zhou, Z. A first-principles study of electronic structure and photocatalytic performance of two-dimensional van der Waals MTe2−As (M = Mo, W) heterostructures. *Int. J. Hydrogen Energy* **2020**, *45* (51), 27089−27097.
(22) Zhang, X.; Zhang, Z.; Wu, D.; Zhang, X.; Zhao, X.; Zhou, Z. Computational Screening of 2D Materials and Rational Design of Heterojunctions for Water Splitting Photocatalysts. *Small Methods* **2018**, *2* (5), 1700359.
(23) Xia, C.; Xiong, W.; Du, J.; Wang, T.; Peng, Y.; Li, J. Universality of electronic characteristics and photocatalyst applications in the two-dimensional Janus transition metal dichalcogenides. *Phys. Rev. B* **2018**, *98* (16), 5424 DOI: 10.1103/PhysRevB.98.165424.
(24) Wang, J.; Shu, H.; Zhao, T.; Liang, P.; Wang, N.; Cao, D.; Chen, X. Intriguing electronic and optical properties of two-dimensional Janus transition metal dichalcogenides. *Phys. Chem. Chem. Phys.* **2018**, *20* (27), 18571−18578.
(25) Zhang, J. L.; Zhao, S.; Han, C.; Wang, Z.; Zhong, S.; Sun, S.; Guo, R.; Zhou, X.; Gu, C. D.; Yuan, K. D.; Li, Z.; Chen, W. Epitaxial Growth of Single Layer Blue Phosphorus: A New Phase of Two-Dimensional Phosphorus. *Nano Lett.* **2016**, *16* (8), 4903−4908.
(26) Zhu, Z.; Tománek, D. Semiconducting Layered Blue Phosphorus: A Computational Study. *Phys. Rev. Lett.* **2014**, *112* (17), 6802 DOI: 10.1103/PhysRevLett.112.176802.
(27) Ding, Y.; Wang, Y. Structural, Electronic, and Magnetic Properties of Adatom Adsorptions on Black and Blue Phosphorene: A First-Principles Study. *J. Phys. Chem. C* **2015**, *119* (19), 10610−10622.
(28) Sun, M.; Chou, J.-P.; Hu, A.; Schwingenschlögl, U. Point Defects in Blue Phosphorene. *Chem. Mater.* **2019**, *31* (19), 8129−8135.
(29) Xiao, J.; Long, M.; Deng, C.-S.; He, J.; Cui, L.-L.; Xu, H. Electronic Structures and Carrier Mobilities of Blue Phosphorus Nanoribbons and Nanotubes: A First-Principles Study. *J. Phys. Chem. C* **2016**, *120* (8), 4638−4646.
(30) Wang, B.-J.; Li, X.-H.; Zhao, R.; Cai, X.-L.; Yu, W.-Y.; Li, W.-B.; Liu, Z.-S.; Zhang, L.-W.; Ke, S.-H. Electronic structures and enhanced photocatalytic properties of blue phosphorene/BSe van der Waals heterostructures. *J. Mater. Chem. A* **2018**, *6* (19), 8923−8929.
(31) Mogulkoc, Y.; Modarresi, M.; Mogulkoc, A.; Alkan, B. Electronic and optical properties of boron phosphide/blue phosphorus heterostructures. *Phys. Chem. Chem. Phys.* **2018**, *20* (17), 12053−12060.
(32) Shu, H.; Wang, Y.; Sun, M. Enhancing electronic and optical properties of monolayer MoSe(2)via a MoSe2/blue phosphorene heterobilayer. *Phys. Chem. Chem. Phys.* **2019**, *21* (28), 15760−15766.
(33) Wang, H.; Zhang, L.; Chen, Z.; Hu, J.; Li, S.; Wang, Z.; Liu, J.; Wang, X. Semiconductor heterojunction photocatalysts: design, construction, and photocatalytic performances. *Chem. Soc. Rev.* **2014**, *43* (15), 5234−5244.
(34) Kresse, G.; Hafner, J. Ab initiomolecular dynamics for liquid metals. *Phys. Rev. B* **1993**, *47* (1), 558−561.
(35) Kresse, G.; Furthmüller, J. Efficient iterative schemes for ab initio total-energy calculations using a plane-wave basis set. *Phys. Rev. B* **1996**, *54* (16), 11169−11186.
(36) Kresse, G.; Joubert, D. From ultrasoft pseudopotentials to the projector augmented-wave method. *Phys. Rev. B* **1999**, *59* (3), 1758−1775.
(37) Blöchl, P. E. Projector augmented-wave method. *Phys. Rev. B* **1994**, *50* (24), 17953−17979.
(38) Perdew, J. P.; Burke, K.; Ernzerhof, M. Generalized Gradient Approximation Made Simple. *Phys. Rev. Lett.* **1996**, *77* (18), 3865−3868.
(39) Krukau, A. V.; Vydrov, O. A.; Izmaylov, A. F.; Scuseria, G. E. Influence of the exchange screening parameter on the performance of screened hybrid functionals. *J. Chem. Phys.* **2006**, *125* (22), 224106.
(40) Monkhorst, H. J.; Pack, J. D. Special points for Brillouin-zone integrations. *Phys. Rev. B* **1976**, *13* (12), 5188−5192.
(41) Grimme, S. Semiempirical GGA-type density functional constructed with a long-range dispersion correction. *J. Comput. Chem.* **2006**, *27* (15), 1787−99.
(42) Grimme, S.; Antony, J.; Ehrlich, S.; Krieg, H. A consistent and accurate ab initio parametrization of density functional dispersion correction (DFT-D) for the 94 elements H-Pu. *J. Chem. Phys.* **2010**, *132* (15), 154104.

https://doi.org/10.1021/acsomega.2c01977
ACS Omega 2022, 7, 37061−37069

(43) Nosé, S. A unified formulation of the constant temperature molecular dynamics methods. *J. Chem. Phys.* **1984**, *81* (1), 511−519.
(44) Mogulkoc, Y.; Modarresi, M.; Mogulkoc, A.; Ciftci, Y. O. Electronic and optical properties of bilayer blue phosphorus. *Comput. Mater. Sci.* **2016**, *124*, 23−29.
(45) Ni, M.; Leung, M. K. H.; Leung, D. Y. C.; Sumathy, K. A review and recent developments in photocatalytic water-splitting using TiO2 for hydrogen production. *Renew. Sust. Energy Rev.* **2007**, *11* (3), 401−425.
(46) Ji, Y.; Yang, M.; Lin, H.; Hou, T.; Wang, L.; Li, Y.; Lee, S.-T. Janus Structures of Transition Metal Dichalcogenides as the Heterojunction Photocatalysts for Water Splitting. *J. Phys. Chem. C* **2018**, *122* (5), 3123−3129.
(47) Bai, Y.; Guan, R.; Zhang, H.; Zhang, Q.; Xu, N. Efficient charge separation and visible-light response of two-dimensional Janus group-III monochalcogenide multilayers. *Catal. Sci. Technol.* **2021**, *11* (2), 542−555.
(48) da Silva, R.; Barbosa, R.; Mançano, R. R.; Durães, N.; Pontes, R. B.; Miwa, R. H.; Fazzio, A.; Padilha, J. E. Metal Chalcogenides Janus Monolayers for Efficient Hydrogen Generation by Photocatalytic Water Splitting. *ACS Appl. Nano Mater.* **2019**, *2* (2), 890−897.
(49) Fu, C.-F.; Sun, J.; Luo, Q.; Li, X.; Hu, W.; Yang, J. Intrinsic Electric Fields in Two-dimensional Materials Boost the Solar-to-Hydrogen Efficiency for Photocatalytic Water Splitting. *Nano Lett.* **2018**, *18*, 6312.
(50) Ji, Y.; Yang, M.; Dong, H.; Hou, T.; Wang, L.; Li, Y. Two-dimensional germanium monochalcogenide photocatalyst for water splitting under ultraviolet, visible to near-infrared light. *Nanoscale* **2017**, *9* (25), 8608−8615.
(51) Li, X.; Li, Z.; Yang, J. Proposed Photosynthesis Method for Producing Hydrogen from Dissociated Water Molecules Using Incident Near-Infrared Light. *Phys. Rev. Lett.* **2014**, *112* (1), 018301.
(52) Bernardi, M.; Palummo, M.; Grossman, J. C. Semiconducting Monolayer Materials as a Tunable Platform for Excitonic Solar Cells. *ACS Nano* **2012**, *6* (11), 10082−10089.
(53) Dai, J.; Zeng, X. C. Bilayer Phosphorene: Effect of Stacking Order on Bandgap and Its Potential Applications in Thin-Film Solar Cells. *J. Phys. Chem. Lett.* **2014**, *5* (7), 1289−1293.
(54) Dai, J.; Wu, X.; Yang, J.; Zeng, X. C. AlxC Monolayer Sheets: Two-Dimensional Networks with Planar Tetracoordinate Carbon and Potential Applications as Donor Materials in Solar Cell. *J. Phys. Chem. Lett.* **2014**, *5* (12), 2058−2065.
(55) Cai, X.; Chen, Y.; Sun, B.; Chen, J.; Wang, H.; Ni, Y.; Tao, L.; Wang, H.; Zhu, S.; Li, X.; Wang, Y.; Lv, J.; Feng, X.; Redfern, S. A. T.; Chen, Z. Two-dimensional Blue-AsP monolayers with tunable direct band gap and ultrahigh carrier mobility show promising high-performance photovoltaic properties. *Nanoscale* **2019**, *11* (17), 8260−8269.
(56) Zhang, X.; Chen, A.; Zhang, Z.; Jiao, M.; Zhou, Z. Rational design of C2N-based type-II heterojunctions for overall photocatalytic water splitting. *Nanoscale Adv.* **2019**, *1* (1), 154−161.
(57) Cui, X.; Ren, P.; Deng, D.; Deng, J.; Bao, X. Single layer graphene encapsulating non-precious metals as high-performance electrocatalysts for water oxidation. *Energy Environ. Sci.* **2016**, *9* (1), 123−129.
(58) He, C.; Zhang, J. H.; Zhang, W. X.; Li, T. T. Type-II InSe/g-C3N4 Heterostructure as a High-Efficiency Oxygen Evolution Reaction Catalyst for Photoelectrochemical Water Splitting. *J. Phys. Chem. Lett.* **2019**, *10* (11), 3122−3128.
(59) Qiao, M.; Liu, J.; Wang, Y.; Li, Y.; Chen, Z. PdSeO3Monolayer: Promising Inorganic 2D Photocatalyst for Direct Overall Water Splitting Without Using Sacrificial Reagents and Cocatalysts. *J. Am. Chem. Soc.* **2018**, *140* (38), 12256−12262.

https://doi.org/10.1021/acsomega.2c01977
ACS Omega 2022, 7, 37061−37069